

Article

A Coumarin–Hemicyanine Deep Red Dye with a Large Stokes Shift for the Fluorescence Detection and Naked-Eye Recognition of Cyanide

Dongmei Li ¹, Senlin Peng ¹, Xu Zhou ¹, Lingyi Shen ¹, Xianjiong Yang ¹, Hong Xu ^{1,*}, Carl Redshaw ² , Chunlin Zhang ¹ and Qilong Zhang ^{1,*} 

- ¹ School of Basic Medical Science, Guizhou Medical University, Guiyang 550004, China; 15508509190@163.com (D.L.); pengsenlinyuna@outlook.com (S.P.); zhouxu200003@126.com (X.Z.); shenly@stumail.nwu.edu.cn (L.S.); yangxianjiong@126.com (X.Y.); zcl@gmc.edu.cn (C.Z.)
- ² Chemistry, School of Natural Sciences, University of Hull, Cottingham Road, Hull HU6 7RX, UK; c.redshaw@hull.ac.uk
- * Correspondence: xuhong@gmc.edu.cn (H.X.); gzuqlzhang@126.com (Q.Z.); Fax: +86-851-8817-4017 (H.X.); +86-851-8817-4017 (Q.Z.)

Abstract: In this study, we synthesized a coumarin–hemicyanine-based deep red fluorescent dye that exhibits an intramolecular charge transfer (ICT). The probe had a large Stokes shift of 287 nm and a large molar absorption coefficient ($\epsilon = 7.5 \times 10^5 \text{ L}\cdot\text{mol}^{-1}\cdot\text{cm}^{-1}$) and is best described as a deep red luminescent fluorescent probe with $\lambda_{\text{em}} = 667 \text{ nm}$. The color of probe W changed significantly when it encountered cyanide ions (CN^-). The absorption peak (585 nm) decreased gradually, and the absorption peak (428 nm) increased gradually, so that cyanide (CN^-) could be identified by the naked eye. Moreover, an obvious fluorescence change was evident before and after the reaction under irradiation using 365 nm UV light. The maximum emission peak (667 nm) decreased gradually, whilst the emission peak (495 nm) increased gradually, which allowed for the proportional fluorescence detection of cyanide (CN^-). Using fluorescence spectrometry, the fluorescent probe W could linearly detect CN^- over the concentration range of 1–9 μM ($R^2 = 9913$, $\text{RSD} = 0.534$) with a detection limit of 0.24 μM . Using UV-Vis spectrophotometry, the linear detection range for CN^- was found to be 1–27 μM ($R^2 = 0.99583$, $\text{RSD} = 0.675$) with a detection limit of 0.13 μM . The sensing mechanism was confirmed by ¹H NMR spectroscopic titrations, ¹³C NMR spectroscopy, X-ray crystallographic analysis and HRMS. The recognition and detection of CN^- by probe W was characterized by a rapid response, high selectivity, and high sensitivity. Therefore, this probe provides a convenient, effective and economical method for synthesizing and detecting cyanide efficiently and sensitively.

Keywords: coumarin–hemicyanine; deep red fluorescent dye; large Stokes shift; cyanide



Citation: Li, D.; Peng, S.; Zhou, X.; Shen, L.; Yang, X.; Xu, H.; Redshaw, C.; Zhang, C.; Zhang, Q. A Coumarin–Hemicyanine Deep Red Dye with a Large Stokes Shift for the Fluorescence Detection and Naked-Eye Recognition of Cyanide. *Molecules* **2024**, *29*, 618. <https://doi.org/10.3390/molecules29030618>

Academic Editor: Ugo Caruso

Received: 4 January 2024

Revised: 22 January 2024

Accepted: 25 January 2024

Published: 27 January 2024



Copyright: © 2024 by the authors. Licensee MDPI, Basel, Switzerland. This article is an open access article distributed under the terms and conditions of the Creative Commons Attribution (CC BY) license (<https://creativecommons.org/licenses/by/4.0/>).

1. Introduction

Anion recognition has become one of the most important parts of supramolecular chemistry due to the vital roles played by anions in the environment, chemistry and biology. Additionally, anions have potential applications in sensors, functional materials and transmembrane transport [1]. Among the various anions, cyanide has received widespread attention, as it is involved in the synthesis of fibers, resins and herbicides, electroplating and gold extraction processes [2–5].

Cyanide is a highly toxic substance, and trace amounts of cyanide can be absorbed through the gastrointestinal tract, lungs and skin, leading to lesions and issues within the human respiratory system and central nervous system. Moreover, since the brain tissue is extremely sensitive to oxygen, it is the first to be damaged, which ultimately leads to tissue toxicity hypoxia asphyxiation and loss of consciousness and ultimately death [6]. According to the Analytical Methods of Grain Hygiene Standards, the detection limit of

cyanide in grain was determined to be 0.015 mg/kg, and the detection limit of cyanide in the Hygiene Standards for Drinking Water for Domestic Purposes (GB5749-2006) [7] was set at 0.07 mg/L. According to the literature, the lethal dose of cyanide for adults is 0.5–3.5 mg. Cyanide has a wide range of sources and can be released from natural substances such as cassava, almonds and some fruit seeds, in which it mainly exists in the form of cyanogenic glycoside ligands, such as tapioca glucoside in cassava and bitter amygdalin in bitter almonds [8,9]. These substances produce hydrocyanic acid under the catalytic action of enzymes in the human body, and the cyanogen ions (CN^-) produced by them are the root cause of poisoning. The mechanism of action is the inhibition of cytochrome oxidase, so that the cytochrome system is dysfunctional, which leads to asphyxiation of the organism. Therefore, it is essential to monitor and detect the concentration of cyanide in the environment and in humans in real time.

Currently, conventional methods for the detection of cyanide include spectrometry, chromatography and electrochemical methods [10–13]. However, these methods have the disadvantage of requiring a troublesome and time-consuming pre-treatment of samples, and some of them also rely on expensive instrumentation for detection and have certain limitations in terms of reaction speed and quantification. Fluorescent probes have received widespread attention due to their high sensitivity, speed and environmental compatibility [14,15].

To date, there have been many types of cyanide ion probes reported in the literature, which are mainly classified as bonded fluorescent probes and reactive fluorescent probes, all of which have shortcomings. Although bonded fluorescent probes [16,17] do have the advantages of fast response speeds and good water solubility, they exhibit poor selectivity and are susceptible to the interference of other anions during testing, which is problematic for real-world samples. Reactive fluorescent probes can specifically recognize cyanide without interference from other analytes and congeners, and many fluorescent probes have been developed that can specifically recognize cyanide. However, this type of fluorescent probe is often limited to use in pure organic solvents, and some suffer from slower response speeds [14]. Therefore, the development of new fluorescent probes that can quickly, accurately and efficiently recognize and detect cyanide in real samples is an important research direction.

Fluorescent probes with intramolecular charge transfer (ICT) for the rapid identification and detection of cyanide have been reported in the literature [18,19]. They mainly utilize the nucleophilic addition reaction of the probe with CN^- , which interrupts the ICT action of the probe, leading to the alteration of the photophysical properties of the probe [20–23]. Guo et al. [24], obtained a hybrid coumarin–hemicyanine dye with an ICT effect by reacting 1-methyl-2,3,3-trimethyl-3H-indolium and diethylaminocoumarin-aldehyde. The fluorescent probe recognized CN^- in MeOH-Tris-HCl buffer (10 mM, pH = 9.3, 1:1, *v/v*) with a high selectivity and with proportional fluorescence detection of CN^- and a detection limit of 0.6 μM . Considering that most of the anion recognition was carried out in an aqueous solution, the fluorescent probe was clearly water-soluble. Increasing the water solubility of fluorescent probes is necessary, however, and introducing sulfonate groups into the side chain of the molecule is an effective strategy to increase the water solubility of the molecule [25]. In addition, it is also necessary to increase the sensitivity of the probe. Based on this, we reacted diethylaminocoumarin-aldehyde with 4-(2',3',3'-trimethylindole-1-quaternary ammonium salt)-butane-1-sulfonate to obtain an ICT-effective coumarin–hemicyanine deep red dye. Due to the introduction of sulfonate into the probe, the water solubility of the probe was increased, and it was able to recognize CN^- in dimethyl sulfoxide/PBS (10 mM PBS, pH = 7.40, 1:4, *v/v*) with a high selectivity, and the fluorescence detection limit was 0.24 μM , and the UV-Vis detection limit was 0.13 μM .

Furthermore, the designed probe has the following advantages: (1) the probe has a large Stokes shift; (2) the coumarin–semialanthocyanine dye as a chromophore has a large molar absorption coefficient and a large emission wavelength, which can produce obvious

signals and color changes after interacting with CN^- ions for proportional fluorescence detection and naked-eye recognition; (3) the cationic quaternary ammonium salt as an activating group can accelerate the interaction of cyanide ions with the recognition group ($\text{C}=\text{N}$ double bond); and (4) the introduction of a sulfonic acid group and a quaternary ammonium salt can increase the solubility of the probe molecule in aqueous media, which is favorable for applications in real samples.

2. Results

2.1. Structural Characterization

The structure of probe W was characterized by ^1H and ^{13}C NMR spectroscopy and HRMS. We successfully obtained crystals of probe W and performed a single-crystal X-ray diffraction experiment. The crystal structure of the probe showed that double bonds (*cis* configuration) connect the coumarin and indole to form an electron donor (D)- π -electron acceptor (A)-type structure. The nitrogen atoms on the ring of the indole already formed a quaternary ammonium salt (coumarin contains a diethylamino group), and this has a strong electron-pushing effect, so the probe has an intramolecular charge transfer (ICT) property and an electron effect. Probe W is dark green in color, with a maximum emission wavelength of 667 nm, i.e., a deep red luminescent probe, with a molar absorption coefficient of $\epsilon = 7.5 \times 10^5 \text{ L}\cdot\text{mol}^{-1}\cdot\text{cm}^{-1}$ and a Stokes shift of 287 nm. The coumarin and indole rings are not parallel, and they have a dihedral angle of 13.70° between them, whilst the probe molecules interact with each other to form a dimer through typical hydrogen bonding interactions ($\text{C}25\text{--H}25\text{B}\cdots\text{O}4$, $\text{C}24\text{--H}24\cdots\text{O}4$). Furthermore, the dimer forms typical hydrogen bonding interactions at $\text{C}14\text{--H}14\cdots\text{O}2$, $\text{C}3\text{--H}3\text{A}\cdots\text{O}2$, $\text{C}1\text{--H}1\text{B}\cdots\text{O}2$ with $\text{C}14$, $\text{C}3$ and $\text{C}11$ of an adjacent dimer, respectively, through the $\text{O}2$ atoms of the sulfonate root (hydrogen bonding parameters are provided in Supplementary Table S2), thus expanding into a one-dimensional structure (Figure 1).

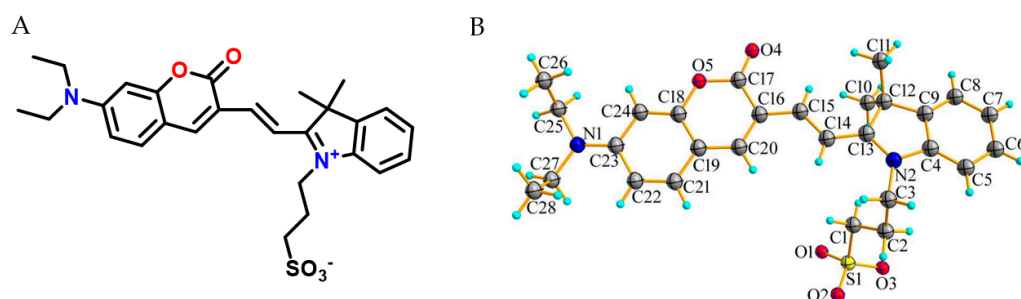


Figure 1. (A) Chemical structure of probe W; (B) thermal ellipsoid plot at 30% level of the asymmetric units of the complexes W.

2.2. Determination of Optimal Experimental Conditions

If the probe can recognize cyanide in an aqueous solution, this will increase its application value. In addition, the pH of the aqueous solution can be controlled by using a buffer solution to exclude the effect of pH, thus making the identification more accurate and reliable. The optimum water content of the probe used in this experiment was determined experimentally.

The compound showed two emission peaks in dimethyl sulfoxide solution. Starting with blue light emission for $\lambda_{\text{em}} = 479 \text{ nm}$, the fluorescence intensity did not change significantly as the water content (FW) increased from 0 to 30% and gradually decreased from 30% to 95%. Secondly, the other emission peak was a deep red emission peak of $\lambda_{\text{max em}} = 667 \text{ nm}$, and the fluorescence intensity decreased significantly when the water content increased from 0 to 20%, and the fluorescence intensity gradually increased to reach the maximum from 20% to 60% and finally decreased again upon increasing the water content to 95% (Figure 2). It emitted red light under irradiation using 365 nm UV light, and a similar phenomenon could be seen in the fluorescence spectrum. Since the fluorescent

probe W is insoluble in water and was not sensitive to the recognition and detection of ions or molecules when the water content was high, a mixture of dimethyl sulfoxide/PBS (10 mM PBS, pH = 7.40, 1:4, *v/v*) was chosen as the recognition environment.

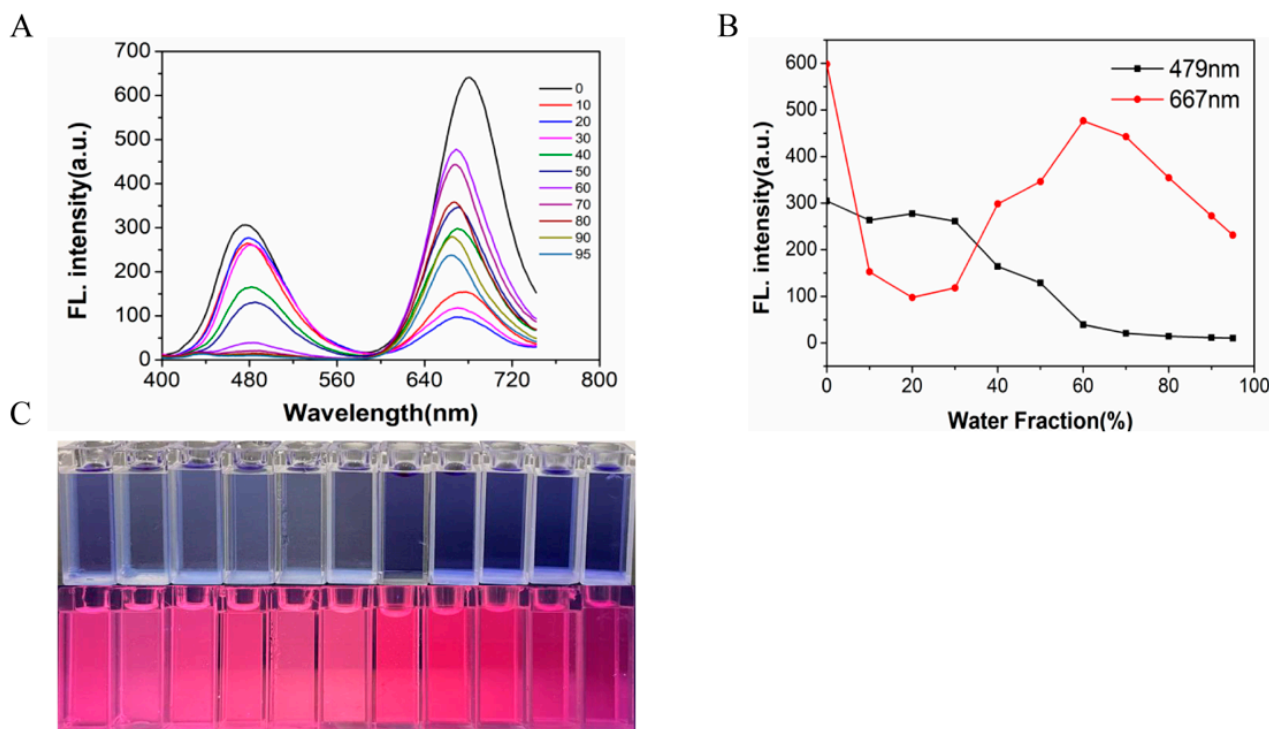


Figure 2. (A) Fluorescence spectra of probe W (10 μ M) using different water contents; (B) effect of water volume fraction (DMSO/PBS system) on fluorescent probe W at maximum emission $\lambda_{em} = 667$ nm, $\lambda_{ex} = 380$ nm, slit: 5/5 nm, voltage: 700 V; fluorescence intensity maps of different water volume fractions at 479 nm/667 nm; (C) fluorescence intensity maps of different water volume fractions under natural light and changes in fluorescence of different water volume fractions under 365 nm UV irradiation.

The pH is also a key parameter that affects the selectivity, sensitivity and detection limit of the probe. Therefore, we experimentally investigated the fluorescence and UV-Vis absorption spectra of probe W over the pH range from 1 to 14.

Firstly, 2.40 mL of PBS buffer of different pH values was added to a 3.00 mL cuvette. Then, 30 μ L of the probe stock solution (1 mM) was added to it, and finally the volume of the solution was made up to 3.00 mL using DMSO, shaken well and left to stand until the system was fully reacted. The effects of the different pH values on probe W were detected by use of a fluorescence spectrophotometer and a UV-Vis spectrophotometer. The detection system consisted of dimethyl sulfoxide/PBS (10 mM PBS, 1:4, *v/v*), and the fluorescence intensities at $\lambda_{ex} = 479$ nm and $\lambda_{em} = 667$ nm tended to stabilize, as did the UV-Vis absorption spectra at 428 nm/585 nm, when in the range from pH = 2 to pH = 8 (Figure 3).

In this experiment, we explored the influence of the water content and pH on the recognition and detection ability of probe W. Dimethyl sulfoxide/PBS buffer (10 mM PBS, pH = 7.40, 1:4, *v/v*) was chosen as the detection system.

The optical stability of probe W-CN⁻ (Supplementary Figure S3) was evaluated over time, and the results showed that the fluorescence spectra and UV-Vis absorption spectra were basically unchanged, indicating that probe W was stable. The fluorescence at $\lambda_{em} = 495$ nm increased rapidly to reach a maximum when probe W-CN⁻ reacted from 0 min to 20 min, and it thereafter remained basically stable upon prolonging the time. The

UV-Vis absorption spectra also exhibited the same behavior, so it was concluded that the optimal reaction time for the recognition of CN^- by probe W was 20 min.

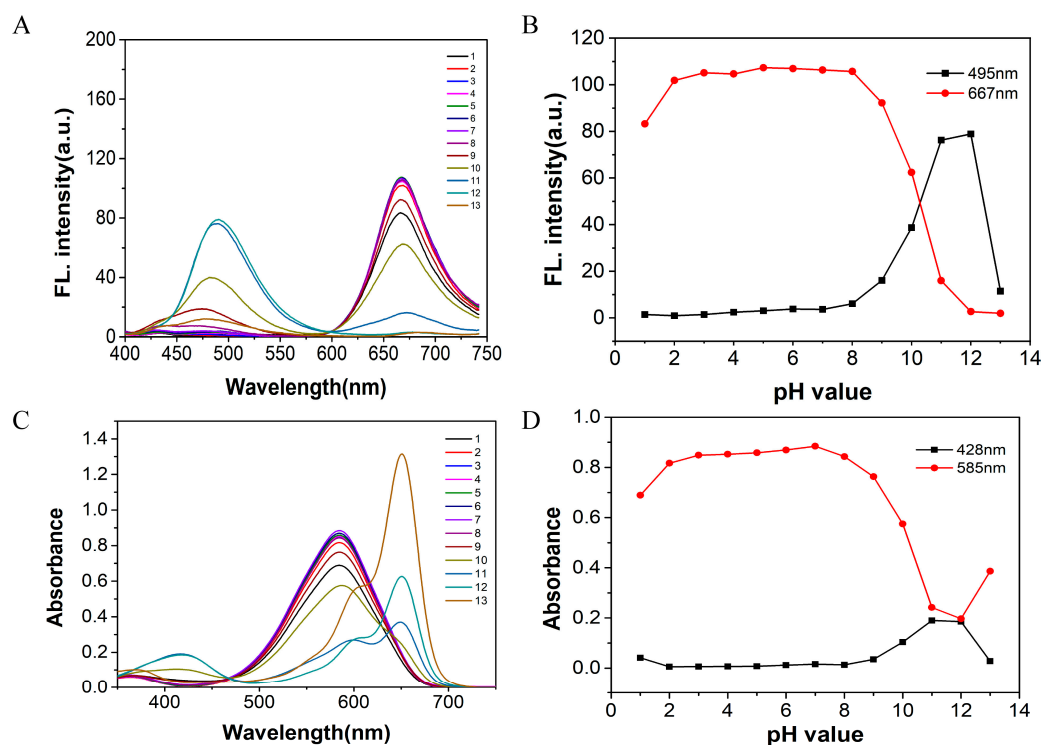


Figure 3. Fluorescence spectra (A) of probe W (10 μM) in the assay system of dimethyl sulfoxide/PBS buffer (10 mM PBS, 1:4, *v/v*) with different pH values; (B) the effect of different pH on the fluorescence of fluorescent probe W at $\lambda_{\text{em}} = 489 \text{ nm}/667 \text{ nm}$, $\lambda_{\text{ex}} = 380 \text{ nm}$, slit: 5/5 nm, voltage: 700 V; (C) UV-Vis spectra; (D) the effect of different pH on the absorbance of UV-Vis light of fluorescent probe W at $\lambda = 428 \text{ nm}/585 \text{ nm}$.

2.3. Anion Sensing Study

A high selectivity and sensitivity of probe W are important parameters for performing water sample detection and *in vivo* studies. Therefore, in order to test its ability to recognize anions, probe W (10 μM) was combined with a variety of anions (such as Br^- , $\text{C}_2\text{O}_4^{2-}$, CH_3COO^- , Cl^- , CN^- , F^- , H_2PO_4^- , HCO_3^- , HPO_4^{2-} , HSO_3^- , I^- , NO_2^- , NO_3^- , PO_4^{3-} , S^{2-} , $\text{S}_2\text{O}_3^{2-}$, SO_3^{2-} and SO_4^{2-}), cations (such as Al^{3+} , Cd^{2+} , Fe^{3+} , Li^+ , Mg^{2+} , Pb^{2+} , Zn^{2+} , Hg^{2+} and Ag^+) and amino-containing small molecules (such as GSH and Cys) in dimethyl sulfoxide/PBS buffer (10 mM PBS, $\text{pH} = 7.40$, 1:4, *v/v*).

After adding anions to the solution containing probe W, a clear change in the color of the solution was observed under irradiation using 365 nm ultraviolet UV light with CN^- , HSO_3^- and S^{2-} . The fluorescence intensity of CN^- was seen to be significantly stronger than that of the other two ions (Figure 4A). The fluorescence spectra also showed that the intensity of the fluorescence emission peak at $\lambda_{\text{em}} = 495 \text{ nm}$ was also significantly stronger when CN^- was added versus the addition of either HSO_3^- or S^{2-} (Figure 4B). When fluorescent probe W detected anions, the fluorescence intensity of CN^- was stronger than that of HSO_3^- or S^{2-} at $\lambda_{\text{ex}} = 380 \text{ nm}$. This was because HSO_3^- or S^{2-} are associated with the C=C nucleophilic addition with probe W, whereas CN^- is associated with a C=N nucleophilic addition reaction. Moreover, fluorescence probes can usually be visualized and employed for detection in a 365 nm UV dark box. Compared with the existing literature, the different recognition results for the different ions may be due to the different excitation wavelengths employed [26].

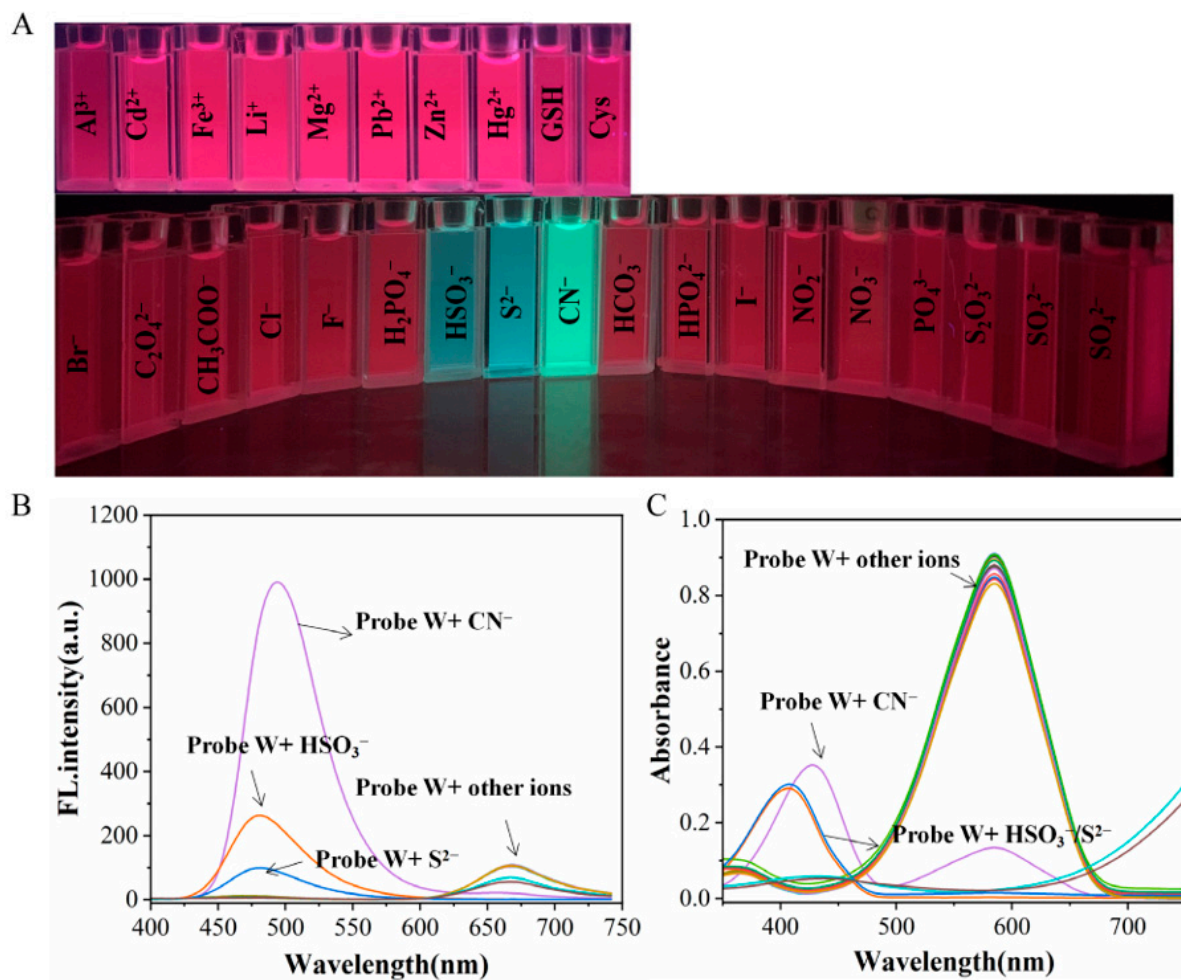


Figure 4. (A) Color changes after addition of different anions and cations under 365 nm UV irradiation; (B) fluorescence spectra of solutions after addition of different anions and cations to probe W (10 μ M) solution in dimethyl sulfoxide/PBS buffer (10 mM PBS, pH = 7.40, 1:4, *v/v*) detection system; (C) $\lambda_{ex}/\lambda_{em}$ = 380 nm/667 nm slit: 5/5 nm, voltage: 670 V and UV-Vis absorption spectrum.

In the UV-Vis spectrum, the maximum absorption peak at $\lambda = 585$ nm decreased significantly after the addition of CN^- , and a new absorption peak appeared at $\lambda = 428$ nm. When HSO_3^- and S^{2-} were added to the solution, the maximum absorption peak at $\lambda = 585$ nm decreased significantly, and a new absorption peak appeared at $\lambda = 408$ nm (Figure 4C). The above experimental results revealed that probe W can selectively recognize and detect anions such as CN^- , HSO_3^- and S^{2-} in the UV-Vis spectra. The fluorescence spectra under excitation at $\lambda_{ex} = 380$ nm and the observation under irradiation using 365 nm UV light revealed that probe W can selectively recognize CN^- with a very good selectivity.

In addition, in order to investigate the competitiveness of probe W in the presence of other competing ions, interference experiments were performed. By observing the change in the fluorescence intensity at $\lambda_{em} = 495$ nm and absorbance at the absorption peak at $\lambda_{ex} = 585$ nm and comparing the solution with and without CN^- , it was found that the fluorescence intensity was higher than that of the other anions when HSO_3^- and S^{2-} were added. Moreover, the absorbance in the UV absorption spectra was lower than that of the other anions, but there was no obvious change in the fluorescence intensity and absorbance upon the addition of other anions and metal cations. The results showed that the coexisting anions and cations had less of an effect on the detection of cyanide. Therefore, the results of the interference experiments showed that probe W has a high specificity, strong selectivity and strong anti-interference ability for the detection of CN^- (Figure 5).

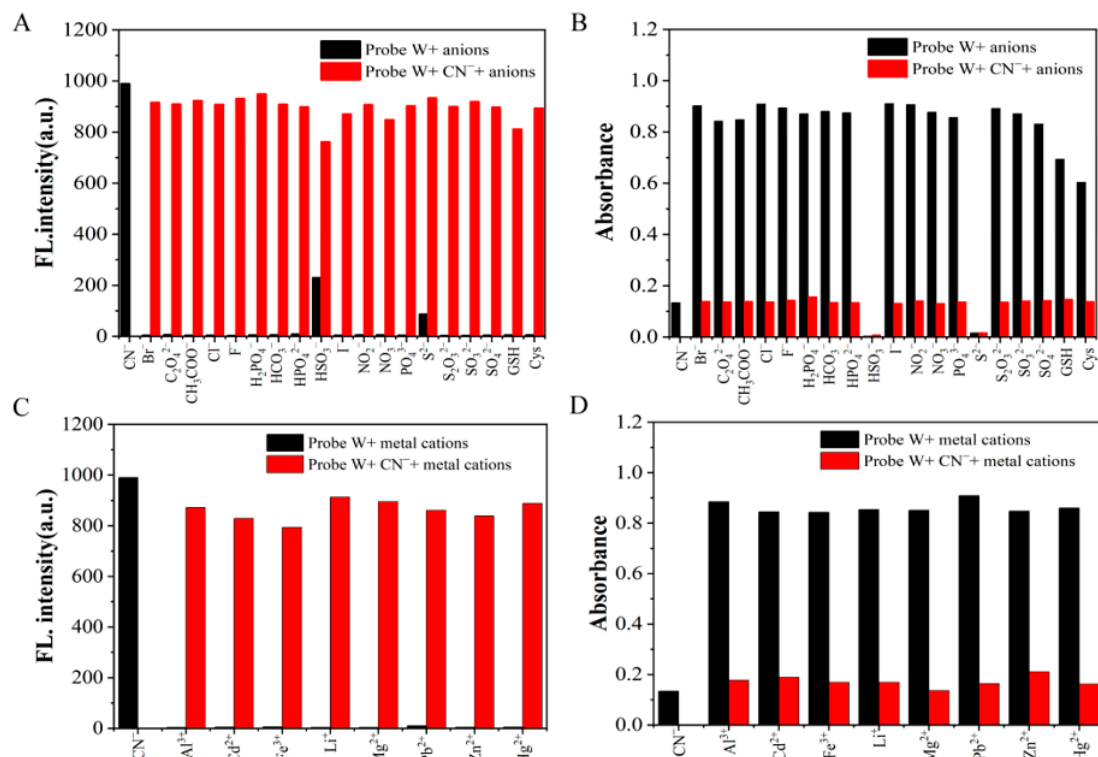


Figure 5. Bar graphs of competition experiments of various anions on (A) fluorescence intensity and (B) absorbance of probe W-CN⁻ mixtures ($\lambda_{ex}/\lambda_{em} = 380 \text{ nm}/667 \text{ nm}$, slit: 5/5 nm, voltage: 670 V). Competition experiment bar graphs of (C) fluorescence intensity and (D) absorbance of various cations against probe W-CN⁻ mixture ($\lambda_{ex}/\lambda_{em} = 380 \text{ nm}/667 \text{ nm}$, slit: 5/5 nm, voltage: 670 V).

2.4. Titration and Detection Limits

On the basis of the above experiments, CN⁻ was gradually added to the solution for fluorescence titration experiments. The fluorescence intensity of probe W at $\lambda_{em} = 495 \text{ nm}$ gradually increased with the increase in the concentration of added CN⁻ ions and finally reached a steady state (Figure 6). In addition, when the concentration of probe W varied between 1–9 μM , a good linear relationship with the concentration of CN⁻ ions ($y = 59.188x + 57.327$, $R^2 = 0.9913$, $\text{RSD} = 0.534$) was observed. In this experiment, the experimental data of the fluorescence titration were utilized for the calculation of the detection limit according to the IUPAC method, i.e., 10 sets of blank samples without CN⁻ were tested under the same conditions, and then the standard deviation (SD) was calculated by the fluorescence intensity at $\lambda_{em} = 495 \text{ nm}$. Finally, according to the formula detection limit = $3\text{SD}/S$ (S is the linear slope in the fluorescence titration experiments), it was calculated that the detection limit of probe W for CN⁻ is 0.24 μM . Compared with other CN⁻ detection probes, probe W has a lower detection limit (Supplementary Table S3).

On the basis of the above experiments, UV titration experiments were carried out by gradually adding CN⁻ to the solution. The absorbance at $\lambda = 585 \text{ nm}$ in the UV-Vis spectrum decreased, and the absorbance at $\lambda = 428 \text{ nm}$ increased with the increase in the concentration of added CN⁻ ions (Figure 7). In addition, when the concentration of probe W varied between 1–27 μM , it showed a good linear relationship with the concentration of CN⁻ ions ($y = 0.0892x + 0.1394$, $R^2 = 0.99583$, $\text{RSD} = 0.675$). The experimental data from the UV titration were utilized for the calculation of the detection limit by the IUPAC method (as above for the ratio of the absorption peaks at $\lambda = 495 \text{ nm}$ and $\lambda = 585 \text{ nm}$). Finally, according to the formula detection limit = $3\text{SD}/S$ (S is the linear slope in the UV titration experiment), the detection limit of probe W for CN⁻ was calculated as 0.13 μM .

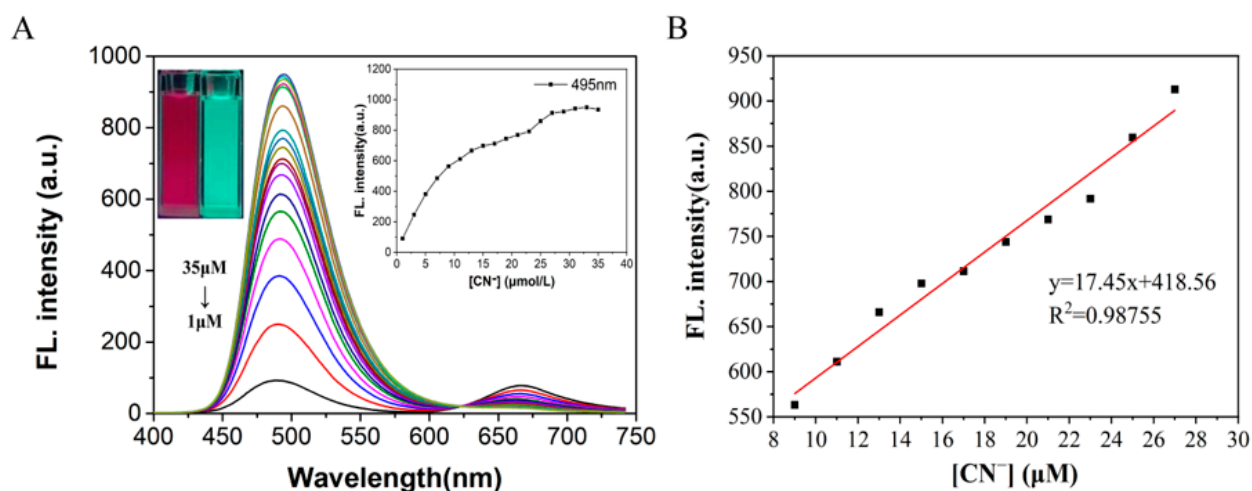


Figure 6. (A) Fluorescence spectra of probe W (10 μM) with the addition of CN^- and (B) linear curves of fluorescence intensity at $\lambda_{\text{em}} = 495 \text{ nm}$ and cyanide concentration (9–27 μM) of the probe solution. Fluorescence intensity curves at $\lambda_{\text{em}} = 495 \text{ nm}$ for different concentrations of cyanide and a photograph of fluorescence color change after irradiation with a 365 nm UV lamp upon completion of the titration (inset in (A)).

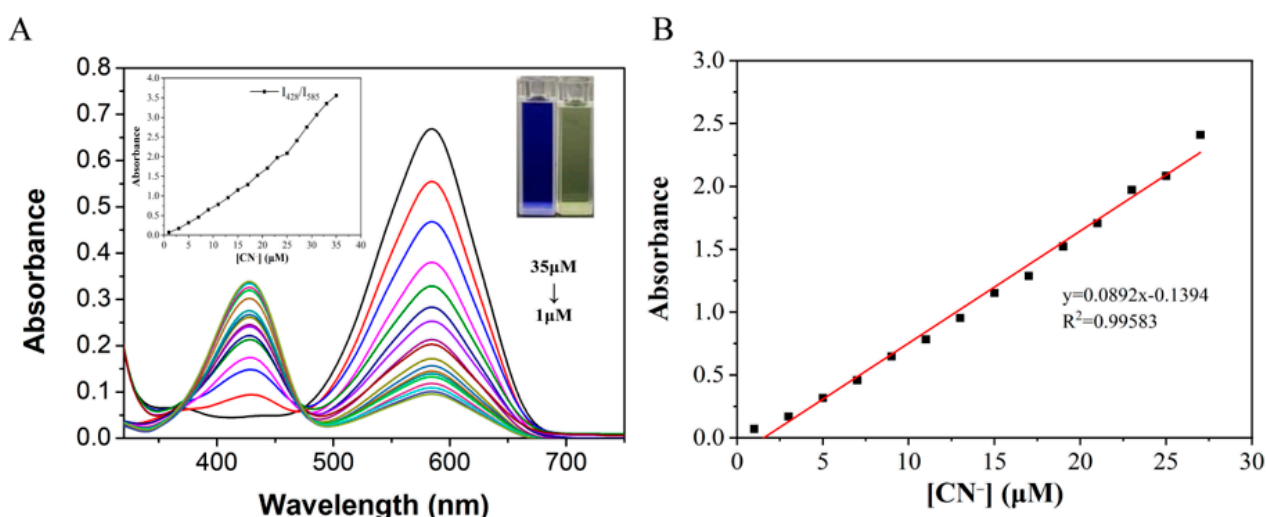


Figure 7. (A) UV-Vis absorption spectra of probe W (10 μM) added with CN^- ; (B) linear curves of absorbance at 428 nm–585 nm of probe solution and cyanide concentration (1–27 μM). Change curve of absorbance ratio at 428 nm–585 nm for different concentrations of cyanide and a photograph of the solution under ambient light illumination showing the changes in the solution upon completion of the titration (inset in (A)).

2.5. Theoretical Calculations and the Possible Mechanism for Detection of CN^-

Based on the existing literature reports and combining the above experimental results, we speculate here on the reaction mechanism of probe W toward recognizing CN^- . Probe W contains a $\text{C}=\text{N}$ double bond, which can easily undergo a nucleophilic addition reaction with CN^- . The color of the probe changed from blue-violet to colorless due to the addition of CN^- to the double bond, destroying the $D-\pi-A$ structure of the probe and weakening the ICT effect. Quantum chemical calculations of the ground and excited states of probe W and its CN^- adducts were carried out using density-functional theory (DFT) and time-varying density-functional theory (TD-DFT), respectively, at the B3LYP/6-311G(d,p) level of theory. The HOMO-LUMO gap of W was 0.09729 eV, whereas the HOMO-LUMO energy level of W-CN^- was 0.12429 eV, indicating that the addition of CN^- hinders the intramolecular

charge transfer. The UV-Vis absorption spectra showed that the absorption peak of W was blue-shifted from 585 nm to 428 nm after the addition of CN^- , which was consistent with the calculated results (Figure 8). The reaction in the solution between probe W and CN^- was verified by high-resolution mass spectrometry (Figure 9). For $[\text{C}_{29}\text{H}_{32}\text{N}_3\text{O}_5\text{S}]^-$: the theoretical value was 534.2068, and the measured value was 534.2067. Subsequently, the CN^- -sensing mechanism of probe W was investigated by NMR spectroscopic titration experiments (Figure 10). The results of the titration showed that the nucleophilic addition of probe W with CN^- generated a neutral compound (Figure 11), which led to a decrease in the electron-absorbing capacity of the indole ring, destroying the conjugated system and inhibiting the ICT process. All the proton signal peaks of probe W were shifted to the high field. In particular, Hk shifted from 9.09 ppm to 8.24 ppm, the proton signal peaks of Hj shifted from 8.29 ppm and 8.27 ppm to 6.90 ppm and 6.85 ppm, the proton signal peaks of Hi shifted from 7.89 ppm and 7.85 ppm to 6.67 ppm and 6.63 ppm and the proton signal peaks of Hf shifted from the triplet peak of 4.68–4.72 ppm to multiplets at 3.02–3.09 ppm. These NMR spectroscopic titration results indicated that a nucleophilic addition reaction between probe W and CN^- had occurred.

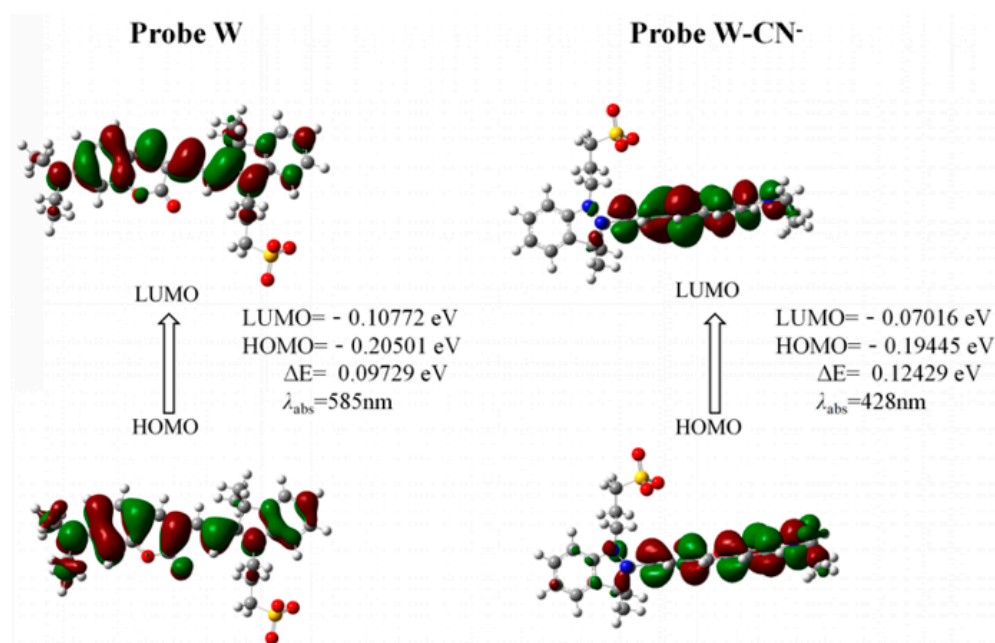


Figure 8. HOMO and LUMO distribution of W and W-CN^- calculated by TD-DFT.

2.6. Applications

One smooth-surfaced and one sprouted green potato were purchased separately and set aside. A total of 0.0800 g of NaOH was added to a beaker containing 20 mL of distilled water and stirred until completely dissolved. A total of 10.00 g of roots and green parts around sprouted potato sprouts were weighed, crushed with a mortar and pestle and transferred to the above NaOH-filled beaker, and distilled water was added to bring the volume up to 30 mL. Then, the system was stirred at 350 rpm for 24 h on a magnetic stirrer protected from light. The stirred solution was removed and centrifuged at 5000 rpm for 30 min, and the supernatant was removed with a 0.22 μm microporous filter to remove large particles that produce fluorescence-dispersed light or absorb light to obtain a cyanide-containing potato solution. A sprouted potato solution containing cyanide was obtained. An unsprouted potato solution was prepared in the same way as above.

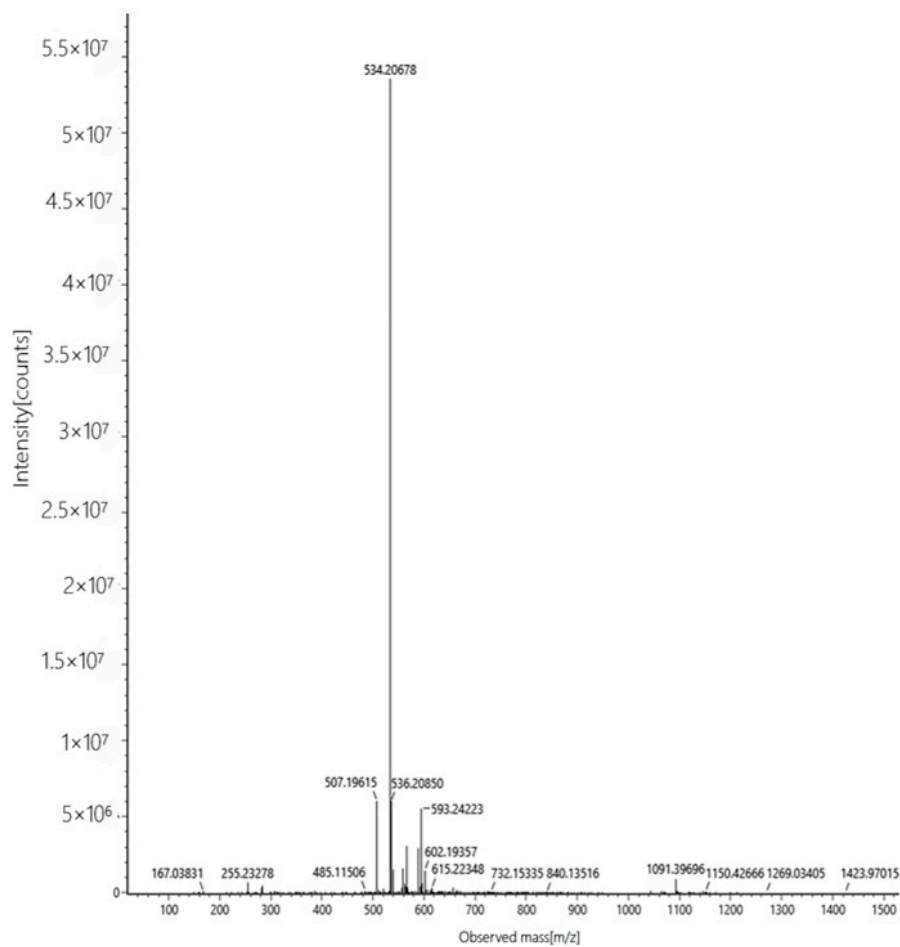


Figure 9. High-resolution mass spectra (HRMS) of the reaction product of probe W upon the addition of CN^- .

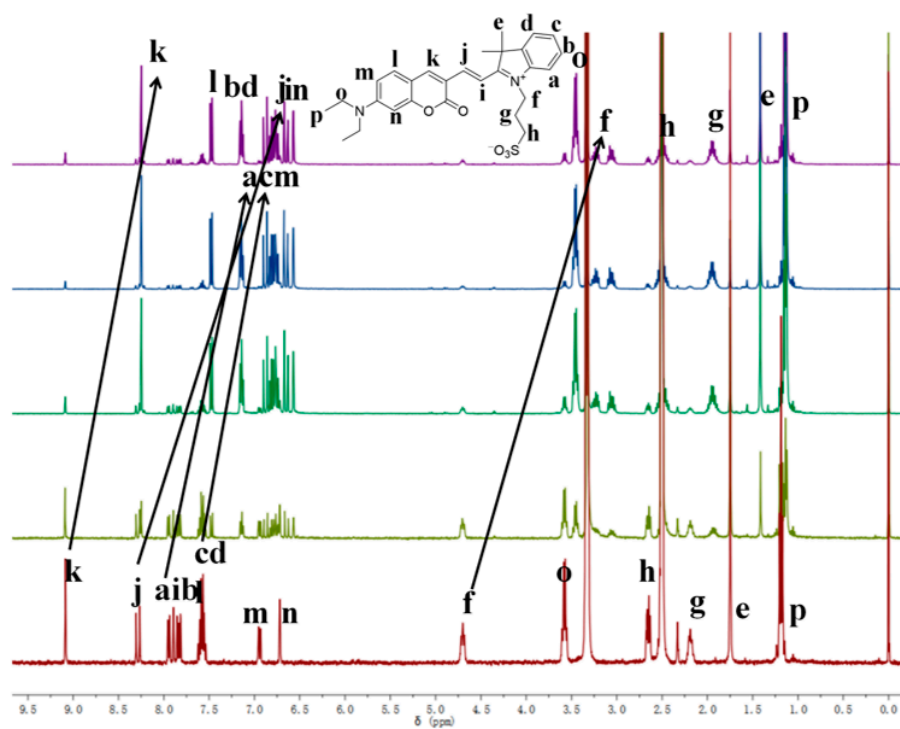


Figure 10. NMR spectral titration of probe W.

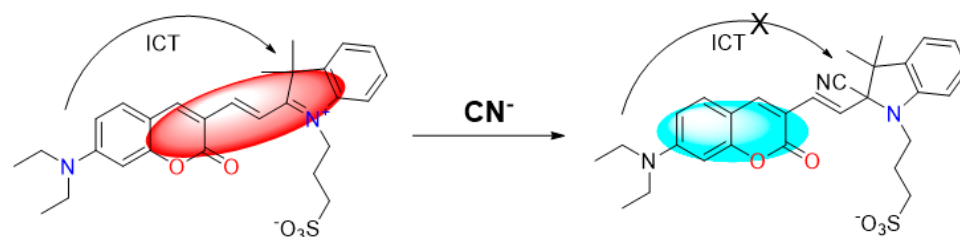


Figure 11. Proposed sensing mechanism of probe W for CN^- .

The measured fluorescence intensity was applied to the standard curve to obtain the CN^- content in the samples and the spiked recoveries. The results in Table 1 show that the spiked recoveries were within the range for both the unsprouted and sprouted potatoes. This indicates that the synthesized fluorescent probe W can be feasibly used to detect CN^- in real samples.

Table 1. Detection of CN^- in unsprouted and sprouted portions of potatoes by probe W.

Sample	Measured Concentration after Spiking (μM)	Sample Concentration (μM)	Spiked Concentration (μM)	Spiked Recovery Rate (%)
Unsprouted potato	2.64	0.65	2.00	99.62
	4.77		4.00	102.58
	6.39		6.00	96.09
Sprouted potato	2.61	0.68	2.00	97.39
	4.92		4.00	105.13
	6.88		6.00	102.99

3. Materials and Methods

3.1. Equipment and Reagents

The following equipment items were employed for characterization: Model VGT-2227QTD Ultrasonic Instrument (Shenzhen Guttehongye Machinery Equipment Co., Ltd., Shenzhen, China); Inova-400 MHz NMR Spectrometer (Varian Company, Palo Alto, CA, USA); CP214 electronic balance (Shanghai Aohaus Instrument Co., Ltd., Shanghai, China); Cary Eclipse-type fluorescence spectrophotometer (Varian Company, Palo Alto, CA, USA), UV-Vis spectrophotometer of UV-2600 (Suzhou Dao Jin Instrument Co., Ltd., Suzhou, China) and pHs-25 pH meter (Chengdu Century Ark Technology Co., Ltd., Chengdu, China).

The following chemicals were employed for the synthetic work: Dimethyl sulfoxide (DMSO), anhydrous ethanol (EtOH), cyanide (as KCN), hydrochloric acid (HCl), metal ions, anions and other reagents were purchased from Aladdin Reagent Co., Ltd. (Shanghai, China). All the chemicals were analytically pure, and no further purification was required during use. The water used to configure the solutions during the experiments was ultrapure water (conductivity 18.2 M Ω cm, U-Pure Ultrapure Technology Co., Ltd., Chengdu, China).

3.2. Synthesis of Fluorescent Probe W

((E)-3-(2-(2-(6-(diethylamino)-3-oxo-3,4-dihydronaphthalen-2-yl)vinyl)-3,3-dimethyl-3H-indol-1-ium-1-yl)propane-1-sulfonate) was synthesized using a one-step process. The synthesis route is shown in Figure 12:

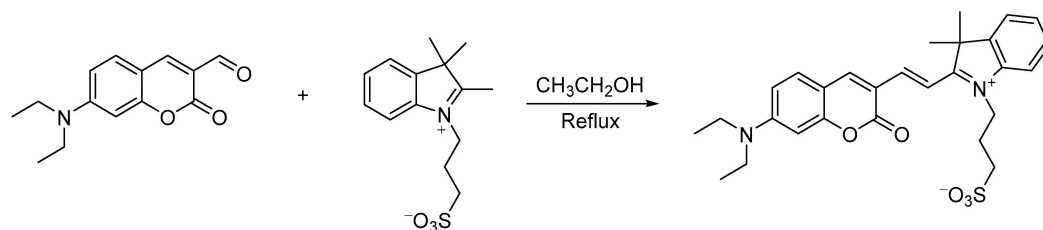


Figure 12. Synthesis route of probe W.

A total of 100 mg (0.5 mM) of diethylaminocoumarin-aldehyde was dissolved with 232 mg (0.55 mM) of 4-(2',3',3'-trimethylindole-1-quatery ammonium salt)-butane-1-sulfonate in 5 mL of anhydrous ethanol, to which 2 drops of piperidine were added, and the reaction was refluxed for 4 h. The reaction was cooled down to room temperature, and a large amount of dark green solid precipitated, which was pump-filtered, and the solid was washed with 5 mL of anhydrous ethanol 3 times. The obtained solid was recrystallized from 10 mL of methanol, and, finally, the dark green solid probe W was obtained. The molecular formula of fluorescent probe W is $C_{29}H_{32}N_3O_5S$. 1H NMR (400 MHz, $DMSO-d_6$) δ 9.09 (s, 1H, Pyran-H), 8.29–8.27 (d, $J = 16.0$ Hz, 1H, CH=CH), 7.94 (d, $J = 7.6$ Hz, 1H, Ar-H), 7.89–7.85 (d, $J = 19.1, 11.6$ Hz, 1H, CH=CH), 7.84–7.82 (d, $J = 16.0$ Hz, 1H, Ar-H), 7.64–7.51 (m, 3H, Ar-H), 6.94 (dd, $J = 9.1, 2.4$ Hz, 1H, Ar-H), 6.72 (d, $J = 2.1$ Hz, 1H, Ar-H), 4.72–4.68 (m, 2H, N^+-CH_2), 3.57 (q, $J = 7.1$ Hz, 4H, $N-CH_2$), 2.64 (s, 2H, $-CH_2SO_3^-$), 2.19 (s, 2H, $-CH_2$), 1.75 (s, 6H, $-CH_3$), 1.18 (t, $J = 7.0$ Hz, 6H, $-CH_3$) (Supplementary Figure S1). ^{13}C NMR (151 MHz, $DMSO-d_6$) δ 179.99, 161.38, 158.90, 154.71, 150.53, 142.71, 140.92, 135.13, 129.54, 128.53, 122.66, 113.32, 113.27, 111.59, 111.21, 108.61, 97.04, 97.02, 51.34, 46.93, 45.75, 45.05, 27.65, 24.73, 12.63 (Supplementary Figure S2). HRMS calculated: 534.2068, found: 534.2067.

3.3. X-ray Crystallography

An APEX 2 CCD diffractometer with graphite-monochromated Mo $K\alpha$ radiation ($\lambda = 0.71073 \text{ \AA}$) in the ω scan mode was used [27]. The structure was solved by a charge-flipping algorithm and refined by full-matrix least-squares methods on F2 [28]. All esds were estimated using the full covariance matrix. Further details are presented in Supplementary Table S1. CCDC: 2307327.

3.4. Preparation of Fluorescent Probe W and Ion Stock Solution

A total of 5.08 mg of the probe was weighed and dissolved in 10 mL of DMSO to prepare a probe stock solution at a concentration of 1 mM. The probe was used as a stock solution for the preparation of the probe. The metal ions of nitrate and the sodium salts of anions (Al^{3+} , Cd^{2+} , Fe^{3+} , Li^+ , Mg^{2+} , Pb^{2+} , Zn^{2+} , Hg^{2+} , Ag^+ , Br^- , $C_2O_4^{2-}$, CH_3COO^- , Cl^- , CN^- , F^- , $H_2PO_4^-$, HCO_3^- , HPO_4^{2-} , HSO_3^- , I^- , NO_2^- , NO_3^- , PO_4^{3-} , S^{2-} , $S_2O_3^{2-}$, SO_3^{2-} and SO_4^{2-}) were accurately weighed and dissolved in PBS to prepare an ionic reserve solution at a concentration of 10 mM. The PBS solution was prepared by accurately weighing 23.00 g of PBS powder and dissolving it in 2 L of ultrapure water at pH 7.20–7.40.

4. Conclusions

In summary, in this study, a one-step method was used to synthesize the target compound probe W using 7-diethylamino-3-formylcoumarin and 4-(2',3',3'-trimethylindole-1-quatery ammonium)-butane-1-sulfonate. Probe W has a large Stokes shift, a large molar absorbance coefficient and a large emission wavelength, and it belongs to the family of deep red luminescence luminescent fluorescent probes. Probe W is capable of producing obvious fluorescent signal changes and color changes upon interacting with CN^- ions, achieving proportional fluorescence detection and naked-eye recognition. The detection limit using the fluorescence spectrum was $0.81 \mu M$ and with a UV-Vis spectra value of $0.13 \mu M$. In addition, probe W was applied to the detection of CN^- in samples of germinated potatoes and showed good results. In this experiment, a probe that can detect CN^- efficiently

and sensitively was synthesized, and an experimental method for the detection of CN^- was established.

Supplementary Materials: The following supporting information can be downloaded at: <https://www.mdpi.com/article/10.3390/molecules29030618/s1>, Figure S1: ^1H NMR spectrum of probe W; Figure S2: ^{13}C NMR spectrum of probe W; Figure S3: Time-varying fluorescence spectra (A) of probe W- CN^- solution in dimethyl sulfoxide/water ($V_{\text{DMSO}}:V_{\text{H}_2\text{O}} = 1:4$, 10 mM PBS buffer) detection system; changes in fluorescence intensities of probe W- CN^- solution over time at the maximum emission at $\lambda_{\text{em}} = 495$ nm, slit: 5/5 nm, voltage: 700 V (B); UV-Vis absorption spectra (C) and the effect of time-dependent UV-Vis absorbance of probe W- CN^- solution at $\lambda = 428/585$ nm (D); Table S1: Summary of crystal data for W; Table S2: Hydrogen-bonding geometries of compound W; Table S3: Comparison data with reported CN^- sensors. References [23,29–35] are cited in the supplementary materials.

Author Contributions: D.L., methodology; S.P., software; X.Z., analyzed the experiment data; L.S. and X.Y., analyzed the X-ray structure; H.X., writing—original draft preparation; C.Z., edited; C.R. and Q.Z., writing—review and editing. All authors have read and agreed to the published version of the manuscript.

Funding: This work was supported by and the National Natural Science Foundation of China (22066007, 22065009) and the Guizhou Provincial Natural Science Foundation (grant number ZK[2022]395, grant number ZK[2023]291).

Institutional Review Board Statement: Not applicable.

Informed Consent Statement: Not applicable.

Data Availability Statement: The datasets presented in this study can be found in online repositories. The names of the repository/repositories and accession number(s) can be found below: <https://www.ccdc.cam.ac.uk/> accessed on 24 January 2024, CCDC: 2307327.

Acknowledgments: C.R. thanks the University of Hull for support.

Conflicts of Interest: The authors declare that the research was conducted in the absence of any commercial or financial relationships that could be construed as a potential conflict of interest.

References

1. Jia, C.D.; Zuo, W.; Zhang, D.; Yang, X.J.; Wu, B. Anion recognition by oligo-(thio)urea-based receptors. *Chem. Commun.* **2016**, 52, 9614–9627. [[CrossRef](#)]
2. Gosi, M.; Marepu, N.; Sunandamma, Y. Cyanine-based Fluorescent Probe for Cyanide Ion Detection. *J. Fluoresc.* **2021**, 31, 1409–1415. [[CrossRef](#)]
3. Li, J.J.; Qi, X.L.; Wei, W.; Liu, Y.C.; Xu, X.; Lin, Q.H.; Dong, W. A “donor-two-acceptor” sensor for cyanide detection in aqueous solution. *Sens. Actuators B Chem.* **2015**, 220, 986–991. [[CrossRef](#)]
4. Abdolhamid, A.; Sohrab, G.; Mohammad, M.K.; Mehdi, A. An interesting spectroscopic method for chromofluorogenic detection of cyanide ion in aqueous solution: Disruption of intramolecular charge transfer (ICT). *J. Chem. Sci.* **2016**, 128, 537–543. [[CrossRef](#)]
5. Li, J.J.; Wei, W.; Qi, X.L.; Zuo, G.C.; Fang, J.K.; Dong, W. Highly selective colorimetric/fluorometric dual-channel sensor for cyanide based on ICT off in aqueous solution. *Sens. Actuators B Chem.* **2016**, 228, 330–334. [[CrossRef](#)]
6. Lou, X.D.; Zhang, Y.; Li, S.; Ou, D.X.; Wan, Z.M.; Qin, J.G.; Li, Z. A new polyfluorene bearing pyridine moieties: A sensitive fluorescent chemosensor for metal ions and cyanide. *Polym. Chem.* **2012**, 3, 1446. [[CrossRef](#)]
7. GB 5749-2006; Standards for Drinking Water Quality. Ministry of Health of the People’s Republic of China, Standardization Administration, Standards Press of China: Beijing, China, 2007.
8. Xu, Z.C.; Chen, X.Q.; Kim, H.N.; Yoon, J.Y. Sensors for the optical detection of cyanide ion. *Chem. Soc. Rev.* **2010**, 39, 127–137. [[CrossRef](#)] [[PubMed](#)]
9. Curtis, A.J.; Grayless, C.C.; Fall, R. Simultaneous determination of cyanide and carbonyls in cyanogenic plants by gas chromatography-electron capture/photoionization detection. *Analyst* **2002**, 127, 1446–1449. [[CrossRef](#)] [[PubMed](#)]
10. Yu, B.; Li, C.Y.; Sun, Y.X.; Jia, H.R.; Guo, J.Q.; Li, K. A new azine derivative colorimetric and fluorescent dual-channel probe for cyanide detection. *Spectrochim. Acta A Mol. Biomol. Spectrosc.* **2017**, 184, 249–254. [[CrossRef](#)] [[PubMed](#)]
11. Shan, D.; Mousty, C.; Cosnier, S. Subnanomolar cyanide detection at polyphenol oxidase/clay biosensors. *Anal. Chem.* **2004**, 76, 178–183. [[CrossRef](#)]
12. Tian, Y.; Dasgupta, P.K.; Mahon, S.B.; Ma, J.; Brenner, M.; Wang, J.H.; Boss, J.R. A disposable blood cyanide sensor. *Anal. Chim. Acta.* **2013**, 20, 129–135. [[CrossRef](#)]

13. Lee, K.S.; Kim, H.J.; Kim, G.H.; Shin, I.; Hong, J.I. Fluorescent chemodosimeter for selective detection of cyanide in water. *Org. Lett.* **2008**, *10*, 49–51. [[CrossRef](#)]
14. Yang, Y.M.; Zhao, Q.; Feng, W.; Li, F.Y. Luminescent chemodosimeters for bioimaging. *Chem. Rev.* **2013**, *113*, 192–270. [[CrossRef](#)]
15. Sukdeb, S.; Amrita, G.; Prasenjit, M.; Sandhya, M.; Sanjiv, K.M.; Suresh, E.; Satyabrata, D.; Amitava, D. Specific Recognition and Sensing of CN[−] in Sodium Cyanide Solution. *Org. Lett.* **2010**, *12*, 3406–3409. [[CrossRef](#)]
16. Wang, S.T.; Chir, J.L.; Yi, J.; Wu, A.T. A turn-on fluorescent sensor for detection of cyanide in aqueous media. *J. Lumin.* **2015**, *167*, 413–417. [[CrossRef](#)]
17. Chen, J.Y.; Zhou, H.Q.; Luo, X.Y.; He, S.H.; Ma, L.J. A reactive fluorescence probe based on naphthalene isothiocyanate for Hg⁺. *J. South China Norm. Univ.* **2018**, *50*, 20–24.
18. Li, L.; Zan, M.H.; Qie, X.W.; Miao, P.; Yue, J.; Chang, Z.M.; Wang, Z.; Bai, F.Q.; Zhang, H.X.; Ferri, J.K.; et al. A highly selective fluorescent probe for cyanide ion and its detection mechanism from theoretical calculations. *Talanta* **2018**, *185*, 1–6. [[CrossRef](#)] [[PubMed](#)]
19. Liu, G.; Shao, J. Anion Ratio Fluorescent Molecular Probe Based on Intramolecular Charge Transfer. *J. Inorg. Chem.* **2011**, *27*, 731. [[CrossRef](#)]
20. Cao, D.X.; Liu, Z.Q.; Verwilt, P.; Koo, S.; Jangjili, P.; Kim, J.S.; Lin, W.Y. Coumarin-Based Small-Molecule Fluorescent Chemosensors. *Chem. Rev.* **2019**, *119*, 10403–10519. [[CrossRef](#)] [[PubMed](#)]
21. Cheng, S.Y.; Pan, X.H.; Shi, M.Y.; Su, T.; Zhang, C.; Zhao, W.; Dong, W. A coumarin-connected carboxylic indolinium sensor for cyanide detection in absolute aqueous medium and its application in biological cell imaging. *Spectrochim. Acta A Mol. Biomol. Spectrosc.* **2020**, *228*, 117710. [[CrossRef](#)]
22. Zhu, Y.L.; Wang, K.N.; Song, W.H.; Dong, B.L.; Zhao, S.F.; Guan, R.F.; Li, Z.P.; Sun, Y.T.; Cao, D.X.; Lin, W.Y. A mitochondria-targeted ratiometric fluorescent probe for endogenous cyanide in biological samples. *Sens. Actuators B Chem.* **2019**, *294*, 283–290. [[CrossRef](#)]
23. Shi, Q.; Wu, S.T.; Shen, L.Y.; Zhou, T.; Xu, H.; Wang, Z.Y.; Yang, X.J.; Huang, Y.L.; Zhang, Q.L. A Turn-On Fluorescent Chemosensor for Cyanide Ion Detection in Real Water Samples. *Front. Chem.* **2022**, *10*, 923149. [[CrossRef](#)]
24. Lv, X.; Liu, J.; Liu, Y.; Zhao, Y.; Sun, Y.Q.; Wang, P.; Guo, W. Ratiometric fluorescence detection of cyanide based on a hybrid coumarin–hemicyanine dye: The large emission shift and the high selectivity. *Chem. Commun.* **2011**, *47*, 12843–12845. [[CrossRef](#)]
25. Li, C.; Iscen, A.; Palmer, L.C.; Schatz, G.C.; Stupp, S.L. Light-Driven Expansion of Spiropyran Hydrogels. *J. Am. Chem. Soc.* **2020**, *142*, 8447–8453. [[CrossRef](#)]
26. Zhang, Q.; Zhang, Y.; Ding, S.S.; Zhang, H.Y.; Feng, G.Q. A near-infrared fluorescent probe for rapid, colorimetric and ratiometric detection of bisulfite in food, serum, and living cells. *Sens. Actuators B Chem.* **2015**, *211*, 377–384. [[CrossRef](#)]
27. Krause, L.; Herbst-Irmer, R.; Sheldrick, G.M.; Stalke, D. Comparison of silver and molybdenum microfocus X-ray sources for single-crystal structure determination. *J. Appl. Crystallogr.* **2015**, *48*, 3–10. [[CrossRef](#)] [[PubMed](#)]
28. Sheldrick, G.M. SHELXT—Integrated space-group and crystal-structure determination. *Acta Crystallogr. Sect. A Found. Adv.* **2015**, *71*, 3–8. [[CrossRef](#)] [[PubMed](#)]
29. Kumar, P.S.; Lakshmi, P.R.; Elango, K.P. An easy to make chemoreceptor for the selective ratiometric fluorescent detection of cyanide in aqueous solution and in food materials. *New J. Chem.* **2019**, *43*, 675–680. [[CrossRef](#)]
30. Long, L.L.; Yuan, X.Q.; Cao, S.Y.; Han, Y.Y.; Liu, W.G.; Chen, Q.; Han, Z.X.; Wang, K. Determination of Cyanide in Water and Food Samples Using an Efficient Naphthalene-Based Ratiometric Fluorescent Probe. *ACS Omega* **2019**, *4*, 10784–10790. [[CrossRef](#)] [[PubMed](#)]
31. Qu, W.J.; Li, W.T.; Zhang, H.L.; Wei, T.B.; Lin, Q.; Yao, H.; Zhang, Y.M. Rapid and Selective Detection of Cyanide Anion by Enhanced Fluorescent Emission and Colorimetric Color Changes at Micromole Levels in Aqueous Medium. *J. Heterocycl. Chem.* **2018**, *55*, 879–887. [[CrossRef](#)]
32. Zhang, Y.X.; Lu, L.Y.; Pan, J.M.; Liu, H.; Ma, J. Preparation a novel phenylcarbazole-based fluorescent sensor for the sensitive and selective detection of CN[−] in water. *Mater. Lett.* **2022**, *313*, 131745. [[CrossRef](#)]
33. Hu, J.H.; Sun, Y.; Qi, J.; Li, Q.; Wei, T.B. A new unsymmetrical azine derivative based on coumarin group as dual-modal sensor for CN[−] and fluorescent “OFF-ON” for Zn²⁺. *Spectrochim. Acta Part A Mol. Biomol. Spectrosc.* **2017**, *175*, 125–133. [[CrossRef](#)] [[PubMed](#)]
34. Pei, P.X.; Hu, J.H.; Chen, Y.; Sun, Y.; Qi, J. A novel dual-channel chemosensor for CN[−] using asymmetric double-azine derivatives in aqueous media and its application in bitter almond. *Spectrochim. Acta Part A Mol. Biomol. Spectrosc.* **2017**, *181*, 131–136. [[CrossRef](#)] [[PubMed](#)]
35. Koc, O.K.; Ozay, H. A simple azoquinoline based highly selective colorimetric sensor for CN[−] anion in aqueous media. *Can. J. Chem.* **2017**, *95*, 771–777. [[CrossRef](#)]

Disclaimer/Publisher’s Note: The statements, opinions and data contained in all publications are solely those of the individual author(s) and contributor(s) and not of MDPI and/or the editor(s). MDPI and/or the editor(s) disclaim responsibility for any injury to people or property resulting from any ideas, methods, instructions or products referred to in the content.